Electronic supplementary information (SI)

Determination of accessibility and spatial distribution of chiral Rh diene complexes immobilized on SBA-15 via phosphine-based solid-state NMR probe molecules

Carolin Rieg,[a]‡ Manuel Kirchhof,[b]‡ Katrin Gugeler,[c] Ann-Katrin Beurer,[a] Lukas Stein,[d] Klaus Dirnberger,[d] Wolfgang Frey,[b] Johanna R. Bruckner,[e] Yvonne Traa,[a] Johannes Kästner,[c] Sabine Ludwigs,[d] Sabine Laschat,[b]* and Michael Dyballa[a]*

[a] Institute of Technical Chemistry, University of Stuttgart, 70569 Stuttgart, Germany

[b] Institute of Organic Chemistry, University of Stuttgart, 70569 Stuttgart, Germany

[c] Institute for Theoretical Chemistry, University of Stuttgart, 70569 Stuttgart, Germany

[d] IPOC – Functional Polymers, Institute of Polymer Chemistry, University of Stuttgart, 70569 Stuttgart, Germany

[e] Institute of Physical Chemistry, University of Stuttgart, 70569 Stuttgart, Germany

*Corresponding authors, Email:

sabine.laschat@oc.uni-stuttgart.de

michael.dyballa@itc.uni-stuttgart.de

1. Characterization data on complexes

[RhCl(L1)(PPh_3)]

Synthesis according to GP 2; red solid (79 %); crystallization from a mixture of hexanes / CH_2Cl_2 in the cold; $[\alpha]_D^{20}$ = +4.7° [c = 3 mg/mL, CH_2Cl_2]; ^{1}H NMR (700 MHz, $CDCl_3$): δ = 8.15–8.00 (m, 2H, *m*-Ar*H*), 7.64–7.54 (m, 6H, *m*-Ar$H_{phosphine}$), 7.43–7.28 (m, 12H, *o*-Ar*H*, *p*-Ar*H*, *o*-Ar$H_{phosphine}$, *p*-Ar$H_{phosphine}$), 4.69–4.60 (m, 1H, 3'-H), 4.52–4.38 (m, 2H, 2'-H, 6-H), 4.25–4.20 (m, 1H, 2'-H), 4.19–4.11 (m, 1H, 5-H), 4.00–4.09 (m, 1H, 1-H), 2.98–2.77 (m, 1H, 4-H), 2.39–2.24 (m, 1H, 4'-H), 1.65 (dt, *J* = 6.9, 1.3 Hz, 1H, 7-H), 1.40 (dt, *J* = 6.9, 1.3 Hz, 1H, 7-H), 0.98 (d, *J* = 7.3 Hz, 3H, 5'-H), 0.94 (d, *J* = 7.3 Hz, 3H, 5'-H) ppm; ^{13}C NMR (176 MHz, $CDCl_3$): δ = 167.3 (C-6'), 155.0 (C-1'), 138.0 (*i*-C_{Ar}), 134.5 (d, *J* = 12.1 Hz, *m*-$C_{Ar,phosphine}$), 131.0 (d, *J* = 41.6 Hz, *i*-$C_{Ar,phosphine}$), 130.2 (d, *J* = 2.0 Hz, *p*-$C_{Ar,phosphine}$), 129.9 (*m*-C_{Ar}), 128.3 (d, *J* = 9.9 Hz, *o*-$C_{Ar,phosphine}$), 127.84 (*o*-C_{Ar}), 127.76 (*p*-C_{Ar}), 87.2 (C-3), 68.5 (C-2), 64.4 (C-2'), 59.7 (C-3'), 59.2 (C-5), 58.7 (C-7), 58.0 (C-6), 57.4 (C-1), 46.5 (C-4), 29.5 (C-4'), 18.1 (C-5'), 15.6 (C-5') ppm; ^{31}P NMR (284 MHz, $CDCl_3$): δ = 28.6 (d, *J* = 166 Hz) ppm; FT-IR (ATR): $\tilde{\nu}$ = 3056 (w), 2963 (w), 2919 (w), 2874 (w), 1976 (w), 1775 (s), 1665 (s), 1573 (w), 1481 (m), 1453 (w), 1435 (m), 1385 (m), 1363 (m), 1302 (m), 1290 (m), 1249 (m), 1209 (m), 1144 (w), 1119 (w), 1095 (m), 1077 (w), 1055 (w), 1028 (w), 1013 (w), 998 (w), 979 (w), 911 (m), 882 (w), 857 (w), 807 (w), 729 (s), 694 (vs), 645 (w), 619 (w), 594 (w), 572 (w), 522 (s), 511 (s), 492 (w), 453 (w), 425 (w) cm^{-1}; LRMS (ESI): *m*/*z* = 426.1 [M – Cl – PPh_3]$^+$, 444.1 [M – Cl – PPh_3 + H_2O]$^+$, 688.2 [M – Cl]$^+$; HRMS (ESI): calcd. for [$C_{38}H_{36}NO_3PRh$]$^+$ 688.1482, found [M - Cl]$^+$ 688.1483.

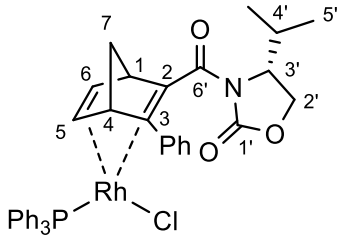

$C_{38}H_{36}ClNO_3PRh$
724.04 g/mol

[RhCl(**L1**)(PPh_3)]

[RhCl(L1)(P(Ad)$_2$(*n*-Bu))]

Synthesis according to GP 2; red solid (94 %); $[\alpha]_D^{20}$ = +1.0° [c = 10 mg/mL, CH_2Cl_2]; ^{1}H NMR (500 MHz, $CDCl_3$): δ = 8.05–7.97 (m, 2H, *m*-Ar*H*), 7.25–7.18 (m, 3H, *p*-Ar*H*, *o*-Ar*H*), 4.73–4.65 (m, 2H, 5-H, 6-H), 4.50 (t, *J* = 8.5 Hz, 1H, 2‘-H), 4.34–4.29 (m, 1H, 1-H), 4.21–4.13 (m, 2H, 4-H, 2‘-H), 3.78–3.58 (m, 1H, 3‘-H), 2.32–2.06 (m, 13H, 4‘-H, P($C_{10}H_{15}$)$_2$), 1.97–1.92 (m, 3H, P($C_{10}H_{15}$)$_2$), 1.89–1.82 (m, 3H, P($C_{10}H_{15}$)$_2$), 1.77–1.48 (m, 17H, 7-H, P(CH_2)$_3$CH$_3$, P($C_{10}H_{15}$)$_2$), 1.45–1.27 (m, 3H, 7-H, P(CH_2)$_3$CH$_3$), 0.98 (d, *J* = 7.3 Hz, 3H, 5‘-H), 0.96–0.89 (m, 6H, 5‘-H, P(CH_2)$_3$CH_3) ppm; ^{13}C NMR (126 MHz, $CDCl_3$): δ = 168.4 (C-6‘), 154.7 (C-1‘), 137.8 (*i*-C_{Ar}), 130.3 (*m*-C_{Ar}), 127.7 (*o*-C_{Ar}), 127.3 (*p*-C_{Ar}), 78.5 (C-3), 64.2 (C-2’), 61.6 (C-2), 59.7 (C-6), 59.6 (C-5), 57.8 (C-7), 57.4 (C-1), 56.3 (C-4), 41.5 (d, *J* = 9.3 Hz, P($C_{10}H_{15}$)$_2$), 40.8 (d, *J* = 9.3 Hz, P($C_{10}H_{15}$)$_2$), 40.5 (C-3’), 40.3 (P($C_{10}H_{15}$)$_2$), 36.7 (d, *J* = 11.4 Hz, P($C_{10}H_{15}$)$_2$), 29.7 (C-4‘), 29.0 (d, *J* = 8.4 Hz, P($C_{10}H_{15}$)$_2$), 28.8 (d, *J* = 8.4 Hz, P($C_{10}H_{15}$)$_2$), 28.4 (P(CH_2)$_3$CH$_3$), 25.8 (d, *J* = 11.4 Hz, P(CH_2)$_3$CH$_3$), 18.1 (C-5’), 17.3 (d, *J* = 14.2 Hz, P(CH_2)$_3$CH$_3$), 15.8 (C-5’), 14.1 (P(CH_2)$_3$$CH_3$) ppm; ^{31}P NMR (162 MHz, $CDCl_3$): δ = 34.7 (d, *J* = 161.2 Hz) ppm; FT-IR (ATR): $\tilde{\nu}$ = 2902 (m), 2847 (m), 1776 (m), 1662 (m), 1450 (w), 1384 (m), 1361 (w), 1343 (w), 1301 (m), 1247 (m), 1207 (m), 1181 (m), 1144 (w), 1120 (w), 1102 (w), 1087 (w), 1056 (w), 1012 (w), 971 (w), 907 (s), 884 (m), 856 (w), 824 (w), 803 (w), 761 (w), 726 (vs), 710 (s), 691 (m), 645 (m), 587 (w), 522 (w), 494 (w), 479 (w), 460 (w), 424 (w) cm^{-1}; LRMS (ESI): m/z = 784.3 [M – Cl]$^+$; HRMS (ESI): calcd. for [$C_{44}H_{60}ClNO_3PRh$]$^+$ 784.3360, found [M - Cl]$^+$ 784.3362.

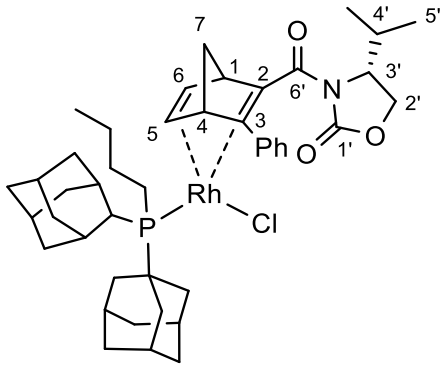

$C_{44}H_{60}ClNO_3PRh$
820.25 g/mol

[RhCl(**L1**)(P(Ad)$_2$(*n*-Bu))]

2. NMR spectra of Rh diene phosphine complexes

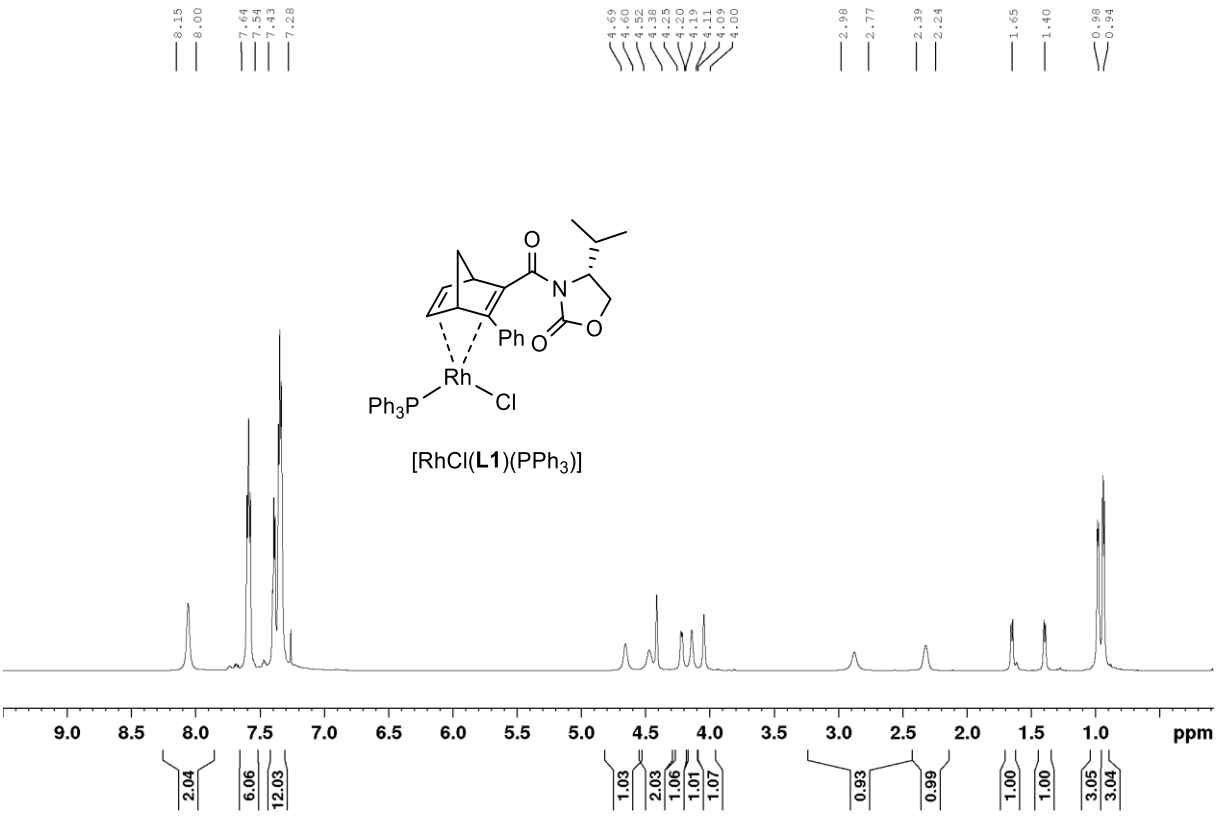

Figure S1. ^{1}H NMR spectrum (700 MHz, $CDCl_3$) of [RhCl(**L1**)(PPh_3)].

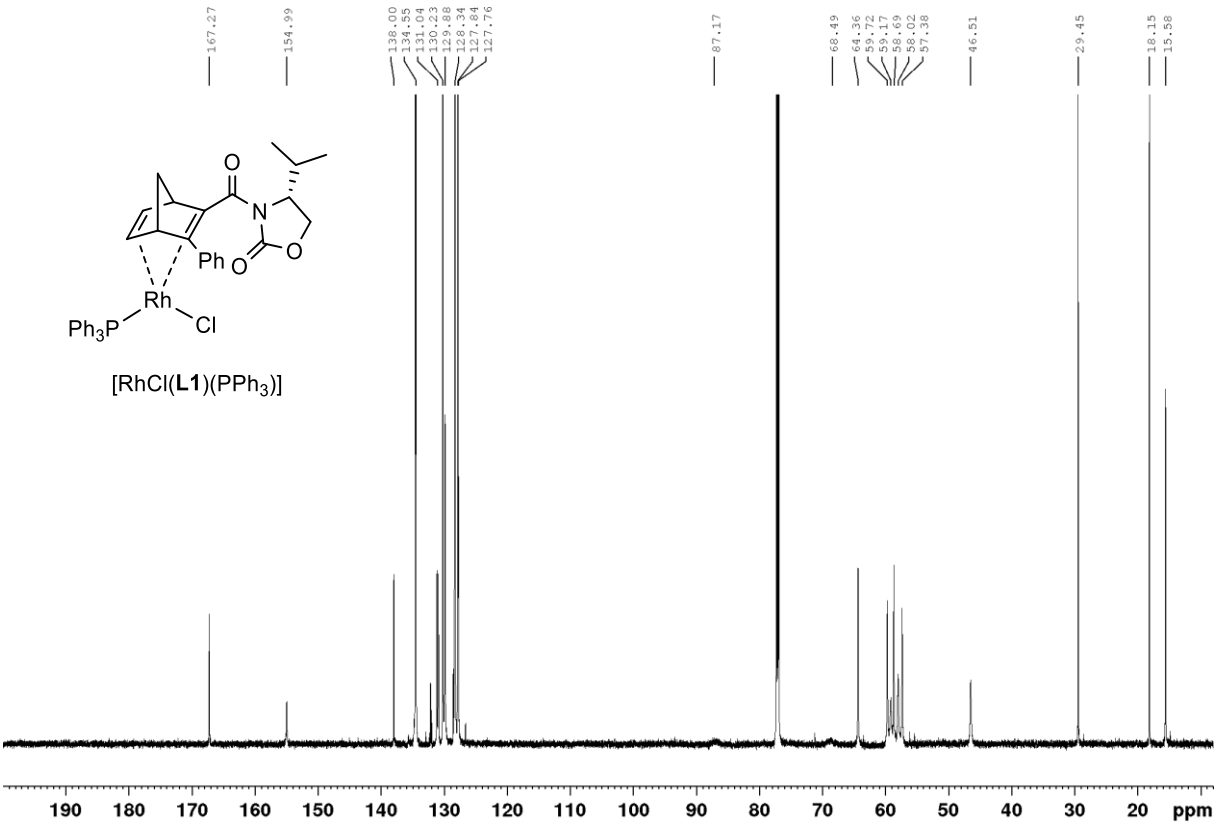

Figure S2. ^{13}C NMR spectrum (176 MHz, $CDCl_3$) of [RhCl(**L1**)(PPh_3)].

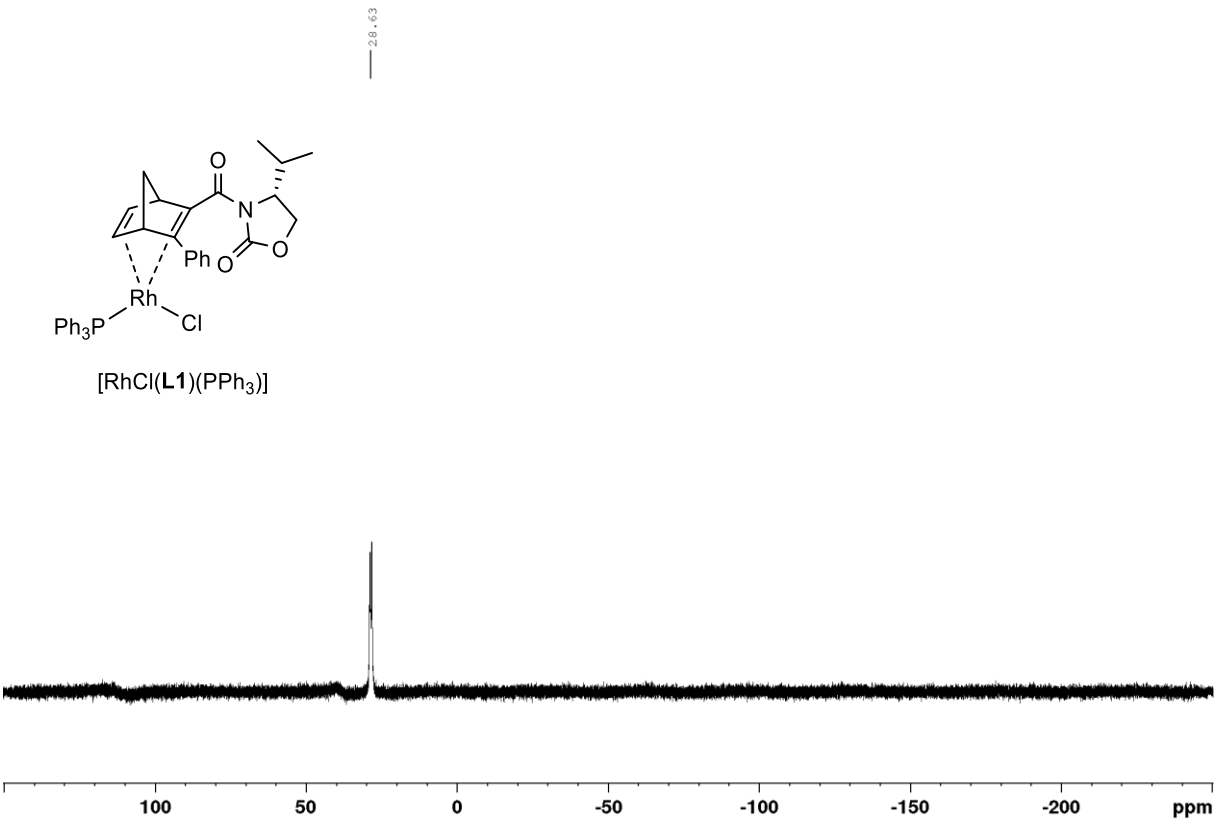

Figure S3. ^{31}P NMR spectrum (284 MHz, $CDCl_3$) of [RhCl(**L1**)(PPh_3)].

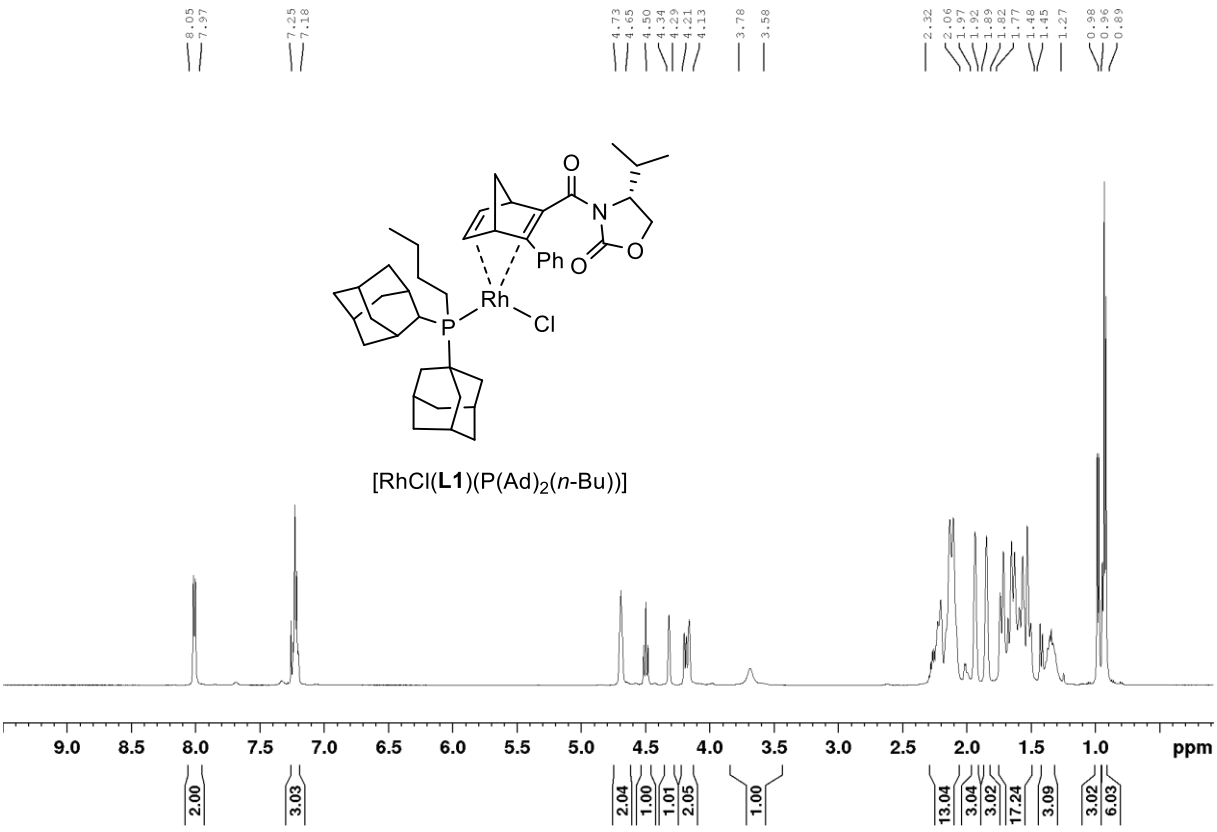

Figure S4. ^{1}H NMR spectrum (500 MHz, $CDCl_3$) of [RhCl(**L1**)(P(Ad)$_2$(*n*-Bu))].

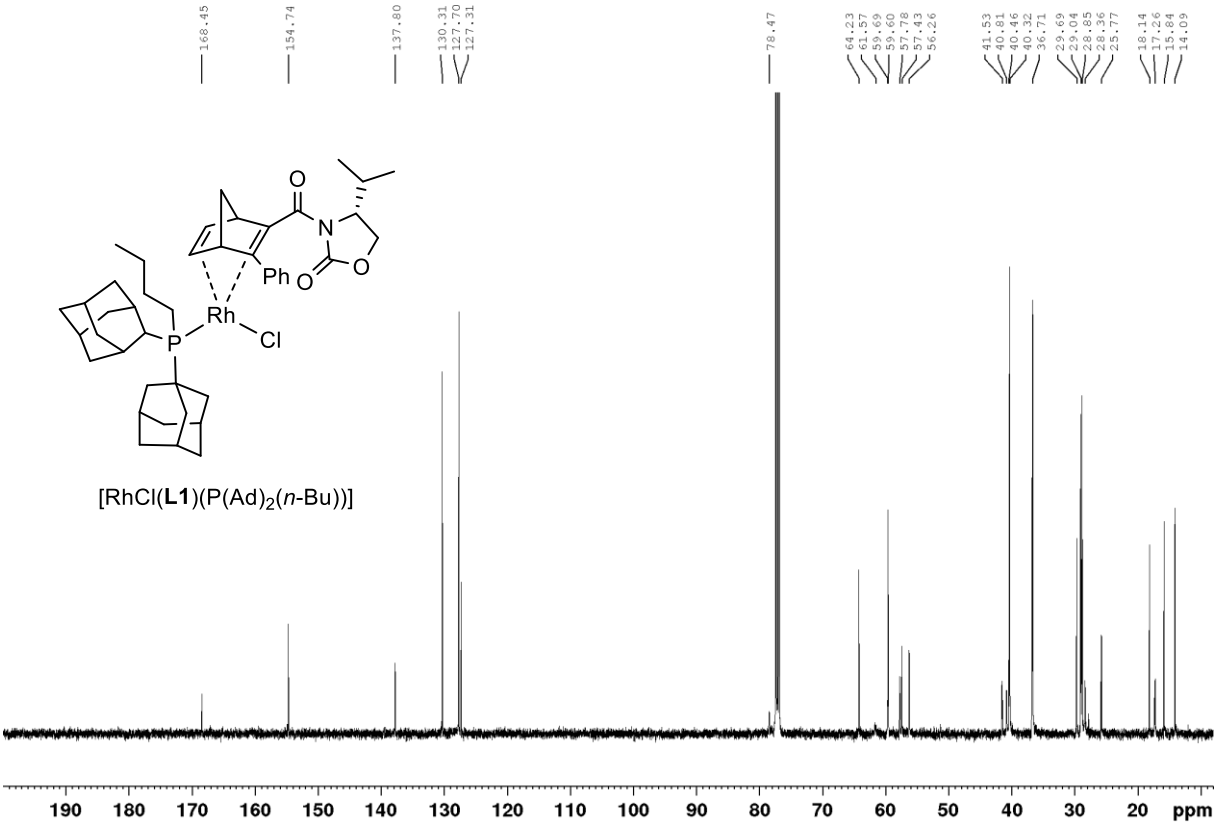

Figure S5. ^{13}C NMR spectrum (126 MHz, $CDCl_3$) of [RhCl(**L1**)(P(Ad)$_2$(*n*-Bu))].

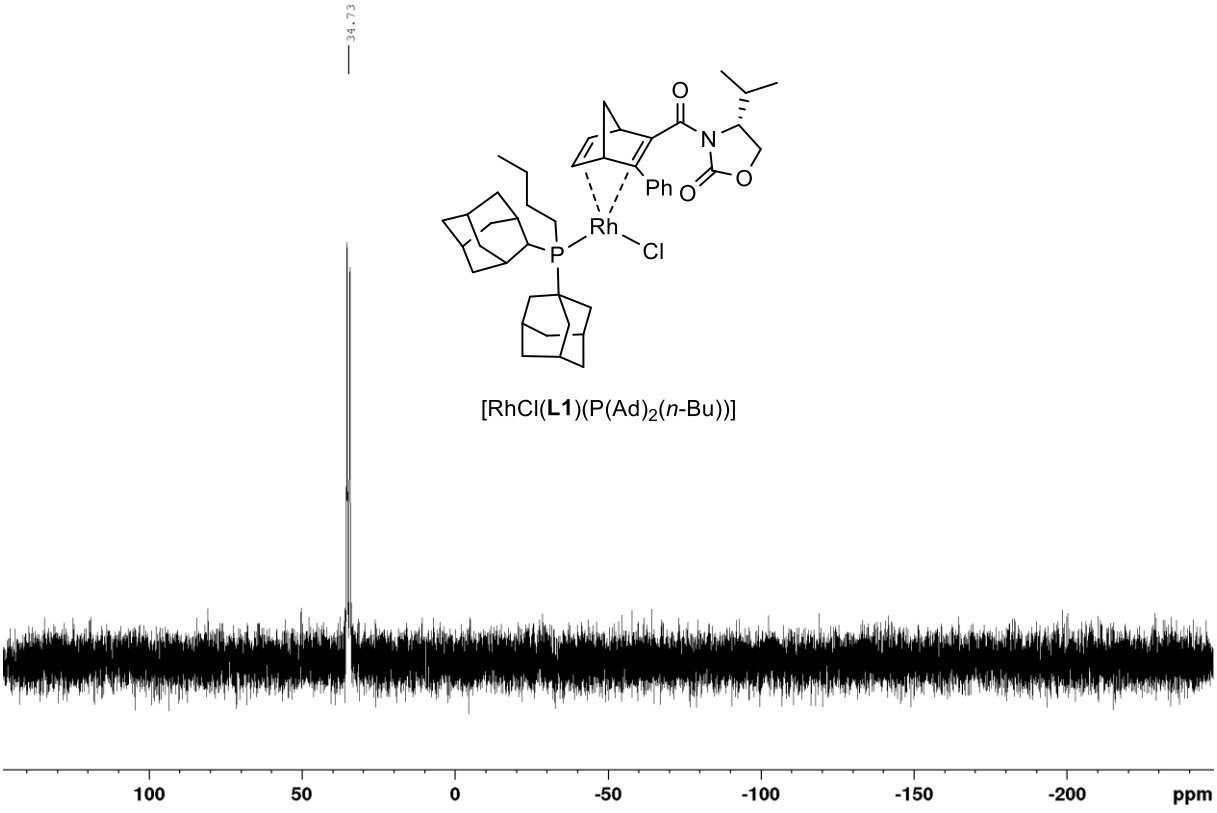

Figure S6. ^{31}P NMR spectrum (162 MHz, $CDCl_3$) of [RhCl(**L1**)(P(Ad)$_2$(*n*-Bu))].

3. Characterization of polymers

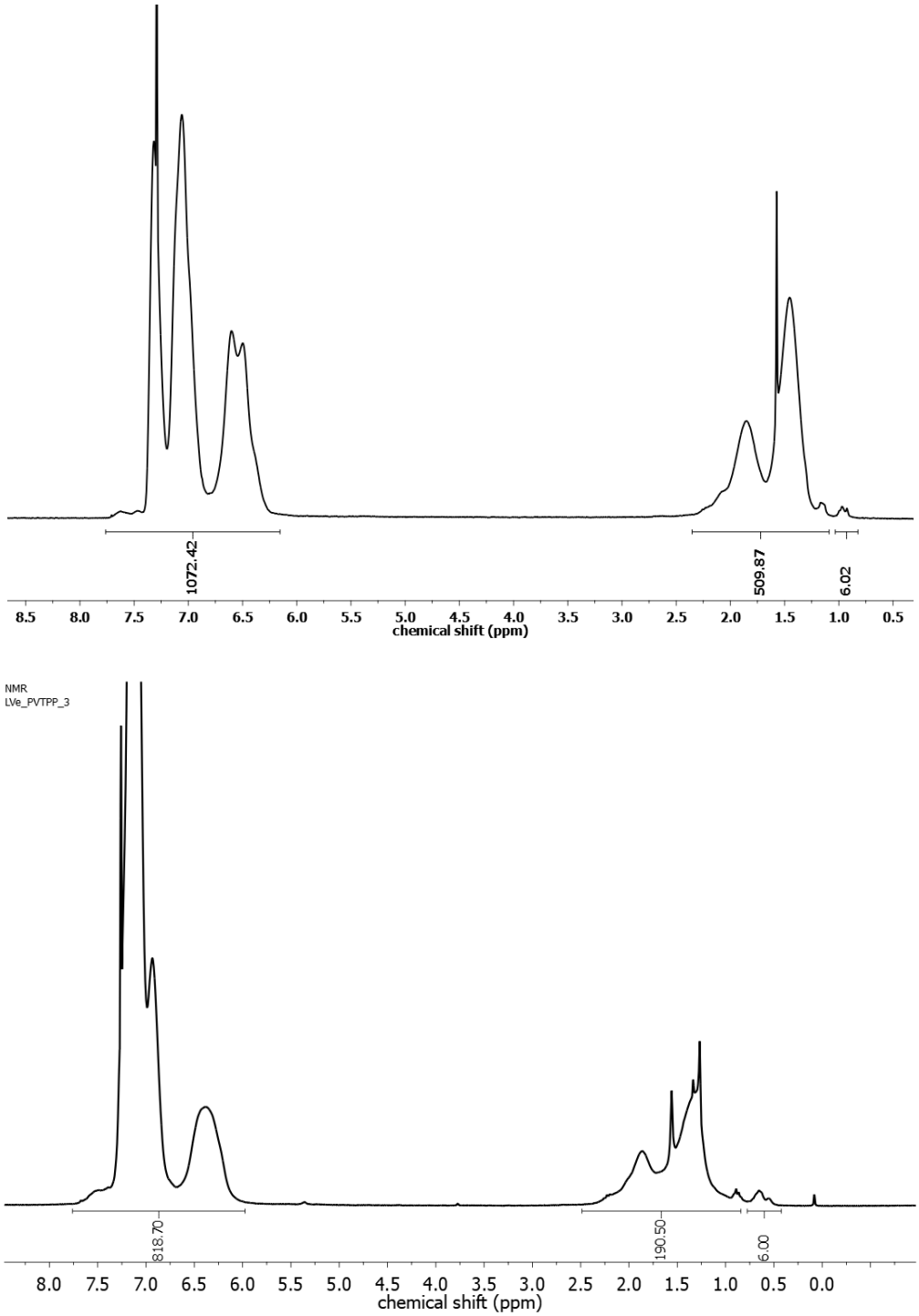

Figure S7. ^{1}H NMR (250MHz, $CDCl_3$) of poly(triphenylphosphine-*co*-styrene) (top) and of poly(triphenylphosphine) (bottom).

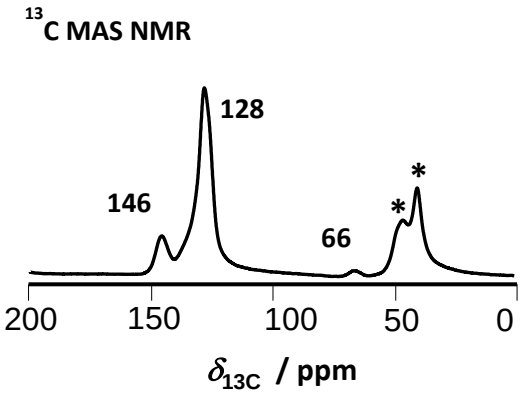

Figure S8. ^{13}C CP MAS NMR of polymer poly(vinyltriphenylphosphine-*co*-styrene). Spinning sidebands are marked by asterisks (*).

4. HPLC chromatograms

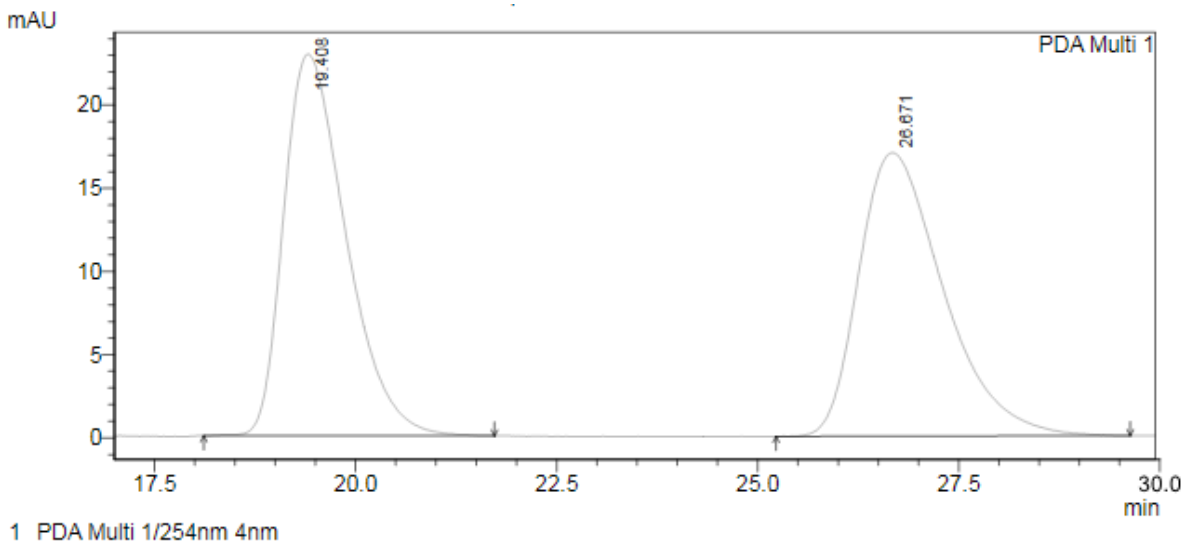

PeakTable

PDA Ch1 254nm 4nm

Peak#	Ret. Time	Area	Height	Area %	Height %
1	19.408	1236222	22949	49.840	57.395
2	26.671	1244135	17036	50.160	42.605
Total		2480357	39985	100.000	100.000

Figure S9. HPLC chromatogram of products (racemic) obtained with $[Rh(COD)Cl]_2$ according to GP 3.

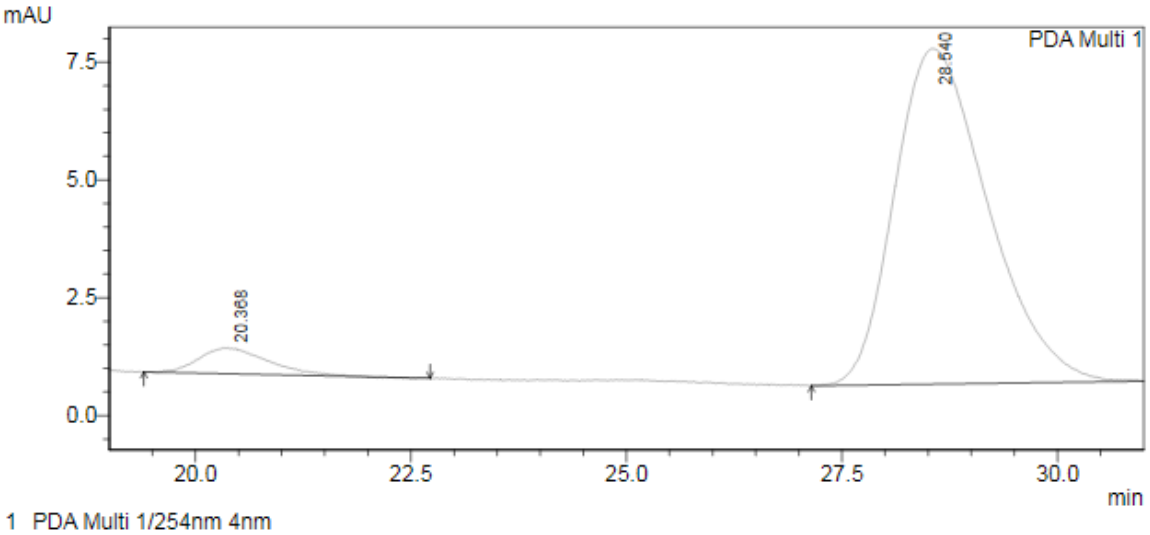

PeakTable

PDA Ch1 254nm 4nm

Peak#	Ret. Time	Area	Height	Area %	Height %
1	20.368	29766	552	5.254	7.187
2	28.540	536761	7123	94.746	92.813
Total		566527	7674	100.000	100.000

Figure S10. HPLC chromatogram of products obtained with [RhCl(**L1**)(PPh_3)] according to GP 3.

5. Computational details

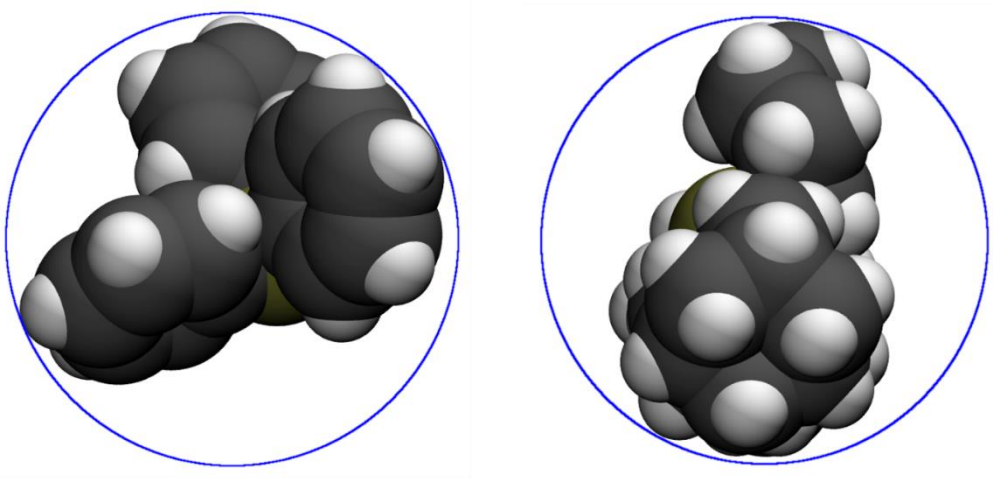

Figure S11. Graphical representation of triphenylphosphine (left) and diadamantylbutylphosphine (right) ligands with their respective van der Waals radii. The ligand sizes were approximated from static visualization of the molecules. For both ligands a molecular diameter of 1.08 nm is found.

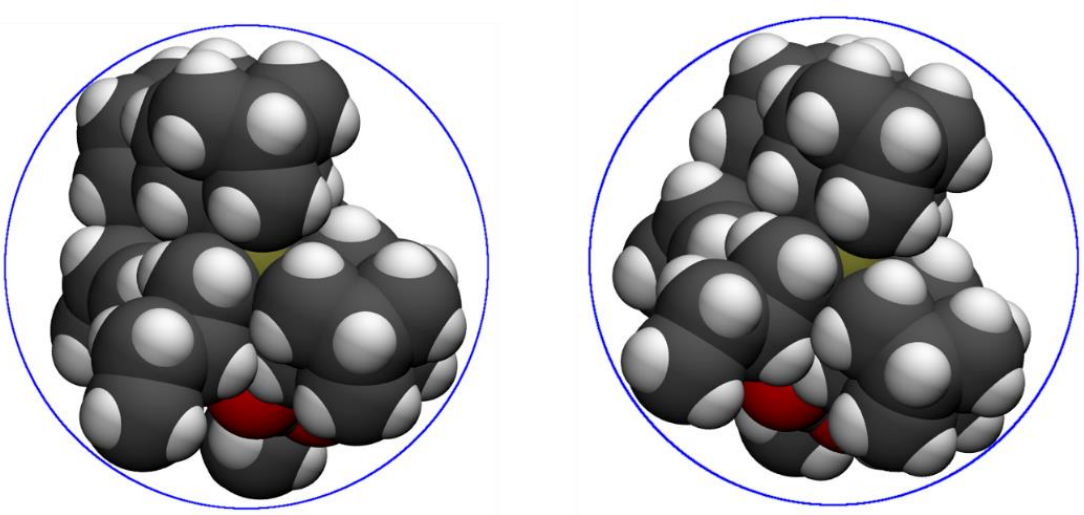

Figure S12. Crystal Structure of [RhCl(**L1**)(P(Ad)$_2$(*n*-Bu))] (cryst.) and [RhCl(**L1**)(P(Ad)$_2$(*n*-Bu))] (DFT opt) with van der Waals radii.

6. Screening of phosphine ligands

Our screening started with the alkyl phosphine P(*n*-Bu)$_3$, which is known to be robust and was verified to bind with Rh (see Figure S13, (a)).[1–3] The formation of the respective Rh diene phosphine complex was verified by ^{31}P NMR spectroscopy, in particular by a chemical shift δ_{31P} = 12.9 ppm and by a doublet with $^1J_{P\text{-}Rh}$ =167 Hz. Due to the low steric bulk of the *n*-butyl groups and the good donor properties of the phosphorous a quantitative binding could be evidenced. However, P(*n*-Bu)$_3$ is air-sensitive, easy to oxidize, and thus not the preferred probe molecule. Next, we tested the arylphosphine PPh$_3$. For the complexation of [RhCl(**L1**)] again a quantitative conversion to the respective Rh diene phosphine complex and a typical chemical shift δ_{31P} = 28.6 ppm were observed. The complex formation could be further confirmed by the coupling constant $^1J_{P\text{-}Rh}$ = 166 Hz (see Figure S13, (b)). In order to test if aryl- or alkyl chains were to be preferred, the complexation with bulky alkyl-arylphosphine P(Ph)$_2$(*t*-Bu) was tested (Figure S13, (c)). Again, full conversion to the respective Rh diene phosphine complex (δ_{31P} = 44.3 ppm, $^1J_{P\text{-}Rh}$ =163 Hz) was observed. However, it should be kept in mind that the introduction of alkyl chains instead of aryl units at the phosphine-P increases the binding affinity as well as the sensitivity against oxygen. Complexation with tri-1-naphthylphosphine resulted only in traces of the Rh diene phosphine complex (δ_{31P} = 21.9 ppm, $^1J_{P\text{-}Rh}$ =156 Hz). Most of the phosphine did not coordinate (δ_{31P} = -33.1 ppm), which is furthermore supported by the absence of any coupling constant $^1J_{P\text{-}Rh}$ visible in the respective spectrum (Figure S13, (d)). The disfavoured coordination might originate from the large steric bulk of the 1-naphthyl substituents in combination with the relatively weak donor properties of the phosphorous atom at this phosphine P(Np)$_3$. Since the bulky *tert*-butyl group was tolerated, subsequently the even more bulky adamantyl (Ad) phosphine P(Ad)$_2$(*n*-Bu) was tested (Figure S13, (e)). The complexation worked smoothly with full conversion as confirmed in the ^{31}P NMR spectrum (δ_{31P} = 34.7 ppm, $^1J_{P\text{-}Rh}$ =161 Hz). We surmised that a large steric bulk is tolerated when strongly coordinating alkyl phosphines are employed. However, for the later immobilization we must keep in mind that we need molecules of up to 7 nm diameter (*vide infra*) to selectively probe the external surface of mesoporous SBA-15. This might lead to strong decreases in sensitivity of the method. To circumvent this problem, we envisaged to use a polymeric probe molecule that is too large to enter mesopores and that can easily be functionalized with phosphine groups at the polymer surface. In two further experiments a homopolymer of vinyltriphenylphosphine (see Figure S13, (f)) and a statistical copolymer of styrene and vinyltriphenylphosphine, PS-*co*-PVPP (Figure S13, (g)) were tested. In both cases full complex formation was observed (polymer peaks are found at higher field, *vide infra*) and only one peak was visible at δ_{31P} = 27.5 ppm. A complex multiplett was observed for the homopolymer, resulting from the proximity of ^{31}P nuclei around the complex, while for the co-polymer a coupling of $^1J_{P\text{-}Rh}$ =161 Hz could be evidenced. We note that in liquid multiple coordination stoichiometries

between surface phosphine groups and Rh complexes might be present that result in two overlapping peaks of mono- and diphosphane-complexes. And since a statistical copolymer was used, it is possible that two peaks occur because the chemical shift of two coordinating VTPP monomer units next to each other is different to the chemical shift of coordinating VTPP units that are separated by styrene monomer units in the polymer backbone.

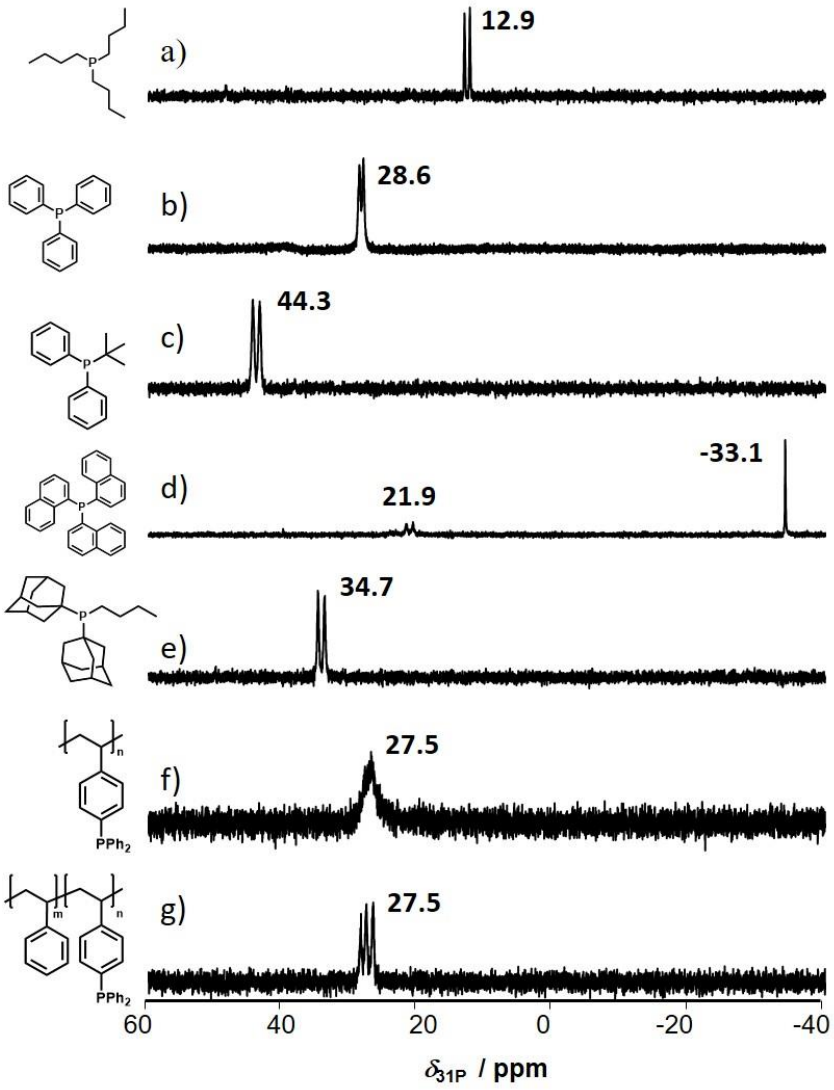

Figure S13: ^{31}P NMR spectra (162 MHz, $CDCl_3$) of the crude products after complexation of [RhCl(**L1**)] with 1 eq. of a) P(*n*-Bu)$_3$, b) PPh_3, c) P(Ph)$_2$(*t*-Bu), d) P(Np)$_3$, e) PAd_2(*n*-Bu), f) poly(vinyltriphenylphosphine), and g) PS-*co*-PVPP.

7. X-Ray crystal structures

For the evaluation of complex sizes, we tried to crystallize some of the complexes from the liquid screening. All attempts to crystallize [RhCl(L1)PPh_3] did not yield suitable single crystals for X-ray analysis. However, the Rh diene phosphine complex [RhCl(L1)($P(Ad)_2$(*n*-Bu))] readily crystallized as red needles and from the crystal structure it became clear that the phosphine coordinated the Rh complex from the less sterically hindered side with no substituents at the norbornadiene (see Figure S14). Interestingly, a strong distortion of the square planar geometry of the Rh(I) complex of 26.2° is observed in the crystal structure (Figure S15, left). In contrast, for the respective Rh diene complex [RhCl(L1)] the distortion is only 5.8° (Figure S15, right). This can be explained by the stronger steric repulsion of the adamantyl substituent and the oxazolidinone moiety as compared to the repulsion of the phenyl moiety and the adamantyl substituent. An overview of the crystal data is presented in Table S1.

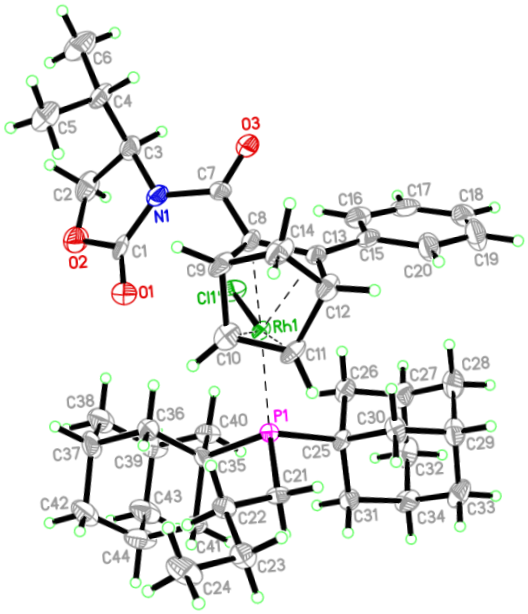

Figure S14: Crystal structure of the Rh diene phosphine complex [RhCl(**L1**)(P(Ad)$_2$(*n*-Bu))].

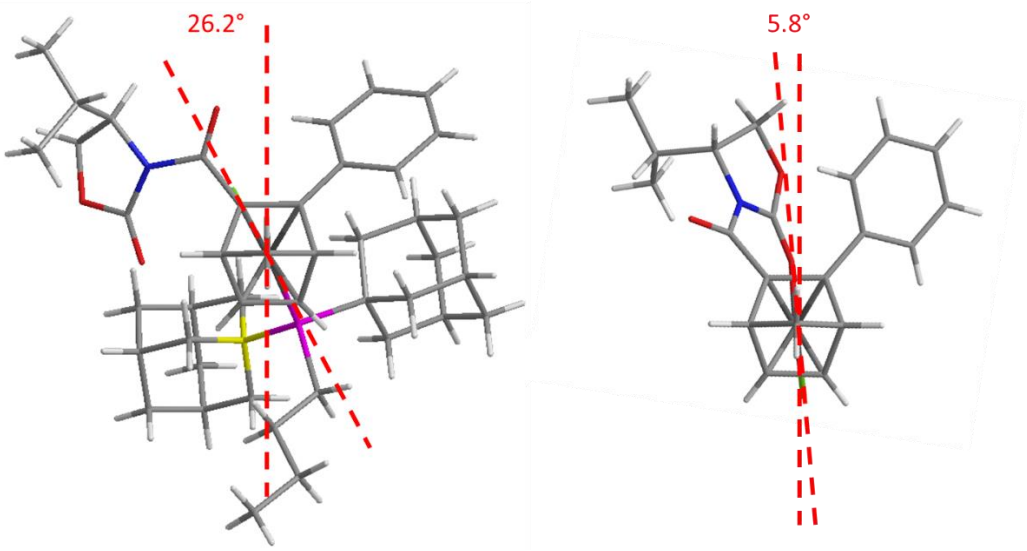

Figure S15. Distortion of square planar geometry of [RhCl(**L1**)(P(Ad)$_2$(*n*-Bu))] (left) and [RhCl(**L1**)]^4 (right).

Table S1. Crystal data and structural refinement details for Rh complex [RhCl(**L1**)(P(Ad)$_2$(*n*-Bu))].[a]

Formula	$C_{44}H_{60}ClNO_3PRh \cdot CHCl_3$
formula weight (g/mol)	939.62
crystal size (mm)	0.192 × 0.160 × 0.137
temperature (K)	140(2)
wavelength λ (Å)	0.71073
crystal system	monoclinic
space group	$P2_1$
unit cell dimension	
a (Å)	10.862(2)
b (Å)	19.566(4)
c (Å)	12.200(2)
α (deg)	90
β (deg)	111.654(10)
γ (deg)	90
V (Å^3)	2409.9(9)
Z	2
D_c (g/cm^3)	1.295
μ (mm^{-1})	0.646
F(000)	980
theta range for data collection	1.796 to 26.437
index ranges	–13≤h≤13, –24≤k≤24, –15≤l≤15
reflection collected/unique	40091 / 9910 [R(int) = 0.0591]
completeness to theta	25.242, 99.9 %
max. and min. transmission	0.7264, 0.6764
refinement methods	Full-matrix least-squares on F^2
data/restraints/parameter	9910 / 25 / 518
GOF on F^2	1.041
R_1, wR_2 [I > 2α(I)]	0.0457, 0.1091
R_1, wR_2 (all data)	0.0575, 0.1155
absolute structure parameter	0.015(12)
extinction coefficient	0.0015(4)
largest diff. peak and hole (e/Å^3)	1.481, –0.665

[a] The cif file was deposited with reference number CCDC 2195463 ([RhCl(**L1**)(P(Ad)$_2$(*n*-Bu))]).

8. SAXS measurements

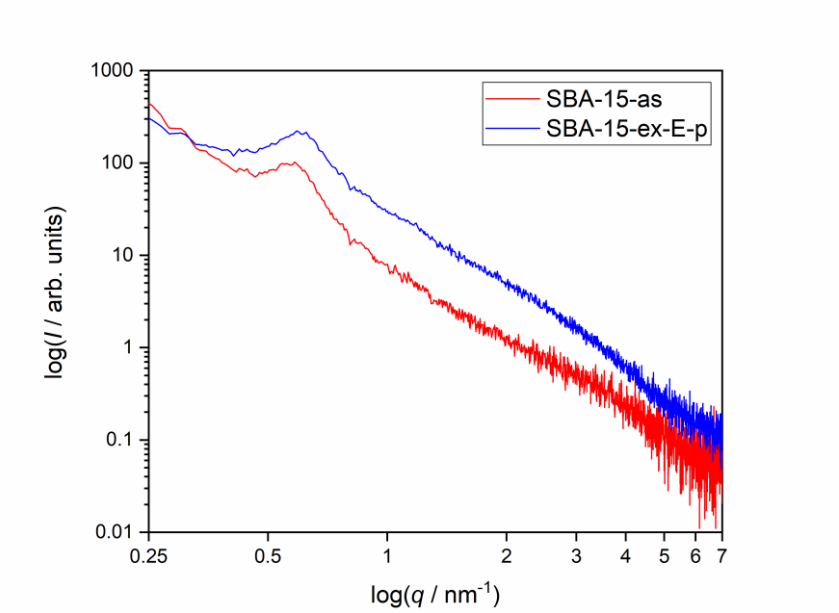

Figure S16: SAXS measurements of template-containing material (SBA-15-as, red) and after passivation of the outer surface and pretreatment at 400°C (SBA-15-ex-E-p, blue) pictured as double logarithmic plot of the scattered intensity *I* vs. the scattering vector *q*.

9. Complexation of [RhCl(L1)] with PPh_3 in the presence of the silica support.

To investigate whether PPh_3 complexation of [RhCl(**L1**)] in the presence of SBA-15 leads to oxidation of PPh_3 to $O{=}PPh_3$ the following experiment was conducted: In a flame-dried flask under a nitrogen atmosphere SBA-15-ex-E-p (0.20 mg) and [RhCl(**L1**)] (10.0 mg, 21.7 µmol) were suspended in degassed CH_2Cl_2 (2 mL) and PPh_3 (5.69 mg, 21.7 µmol) was added. The reaction mixture was stirred for 1 h at room temperature and subsequently filtered over Celite®. The solvent was removed under reduced pressure, the residue was taken up in $CDCl_3$ and a ^{31}P NMR spectrum was recorded (Figure S18).

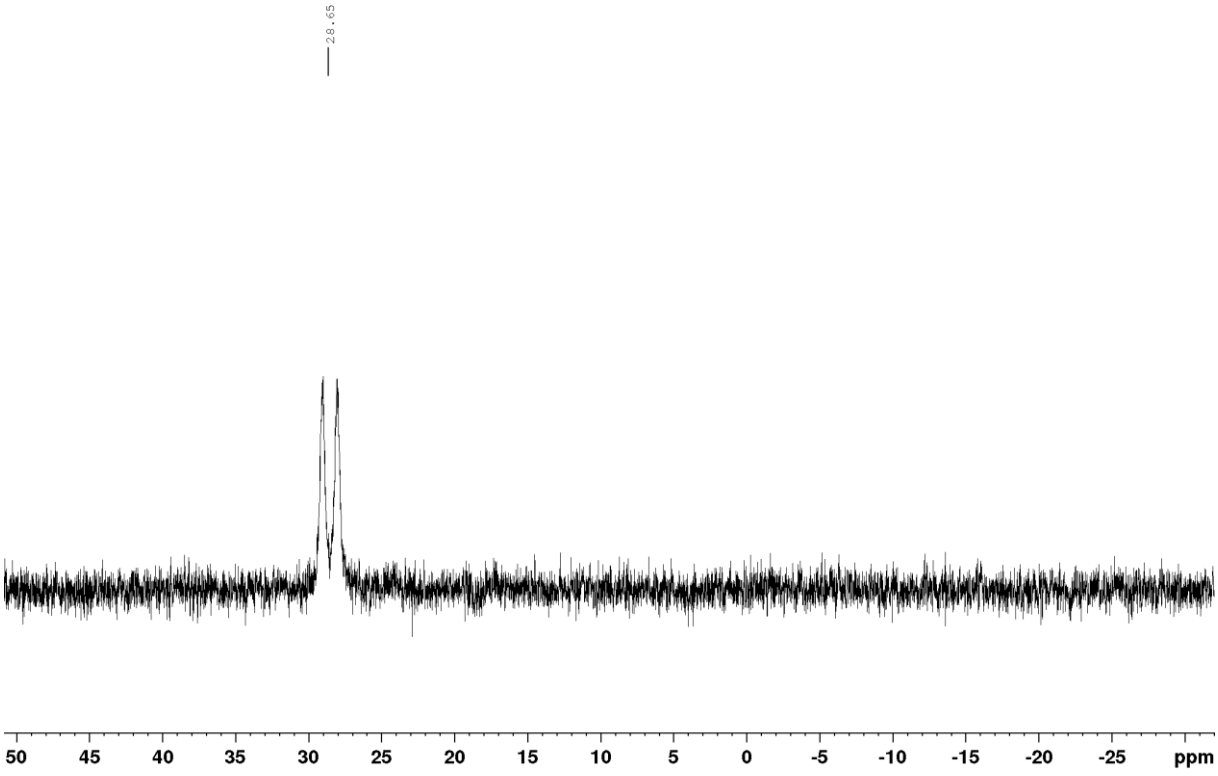

Figure S17. ^{31}P NMR spectrum (162 MHz, $CDCl_3$) of the crude product obtained from PPh_3 complexation of [RhCl(**L1**)] in the presence of SBA-15-ex-E-p.

Only the formation of [RhCl(**L1**)PPh_3] and no $O{=}PPh_3$ was observed in the ^{31}P NMR spectrum.

10. Quantitative ^{31}P MAS NMR spectroscopy on loaded azide groups

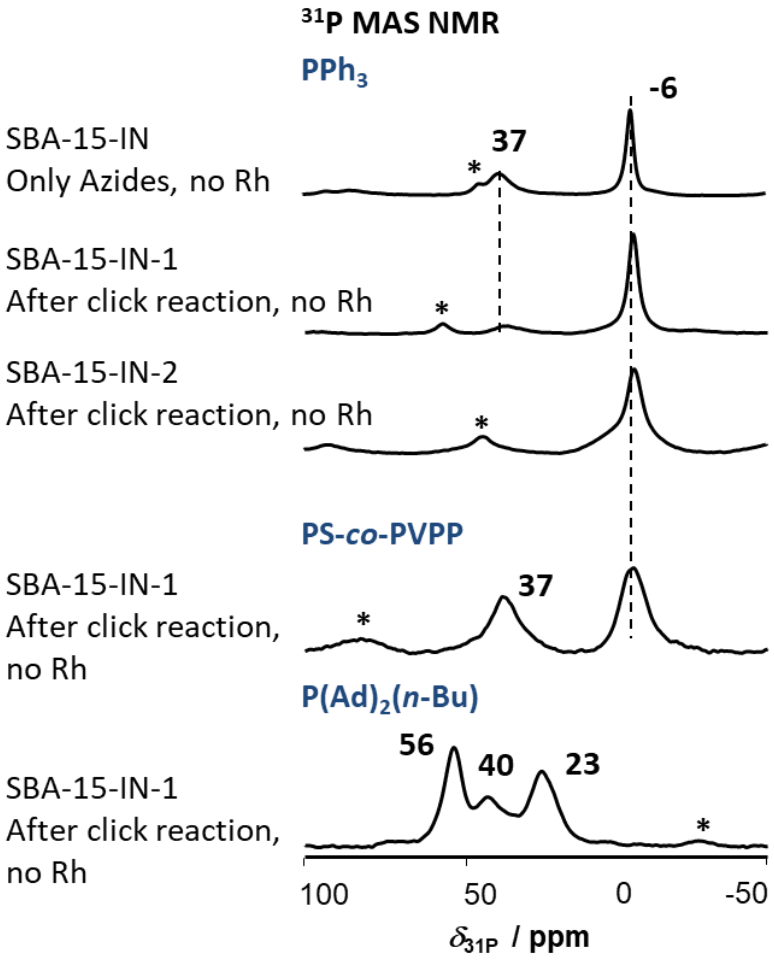

Figure S18. ^{31}P MAS NMR spectra after PPh_3 loading on SBA-15 with (from top to bottom) only azide groups, and after click reaction that lead to SBA-15-IN-1 and SBA-15-IN-2, respectively (no Rh present on herein shown catalysts). Below SBA-15-IN after click reaction that leads to SBA-15-IN-1 (without Rh) and loading with Polymer PS-*co*-PVPP and $P(Ad)_2(n\text{-}Bu)$, respectively. Spinning sidebands are marked by asterisks (*).

11. Stability of [RhCl(L1)PPh$_3$] in the presence of *N*-tosylimines

In catalytic experiments with PPh_3 coordinated catalysts it could be shown that a certain degree of catalytic activity was retained although the PPh_3 should block the required coordination site of the catalyst. To investigate whether the PPh_3 dissociates in the presence of the substrate *N*-tosyl imine **1** the following experiment was conducted: In a flame-dried flask under a nitrogen atmosphere [RhCl(**L1**)PPh_3] (15.7 mg, 21.7 µmol) were suspended in degassed dioxane (3 mL) and *N*-tosyl imine **2** (63.8 mg, 0.22 mmol) was added . The reaction mixture was stirred for 24 h at 60 °C and subsequently the solvent was removed under reduced pressure. The residue was taken up in $CDCl_3$ and a ^{31}P NMR spectrum was recorded (Figure S19).

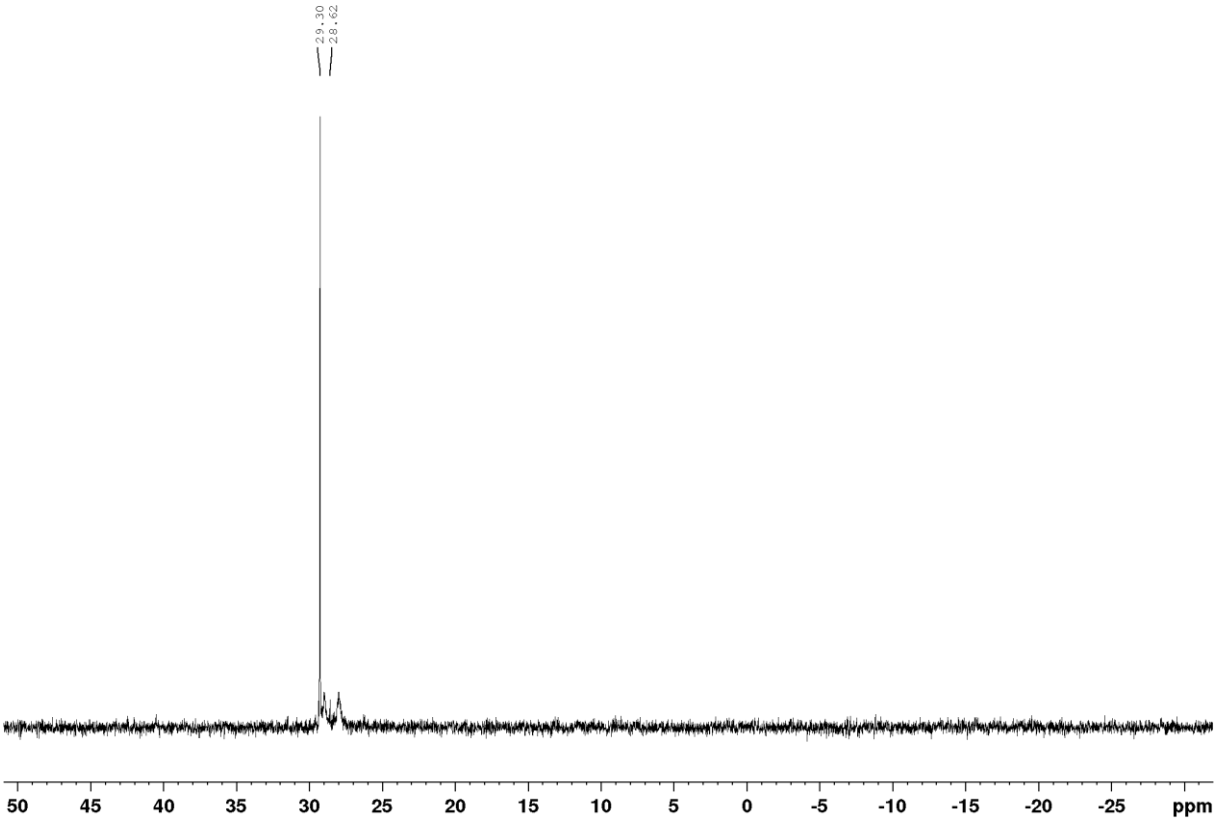

Figure S19. ^{31}P NMR spectrum (162 MHz, $CDCl_3$) of the crude product obtained after stirring [RhCl(**L1**)PPh_3] and *N*-tosyl amine **1** for 24 h in dioxane.

Only small amounts of the original complex [RhCl(**L1**)PPh_3] were found as indicated by the doublet at 28.6 ppm. An additional signal was found at 29.3 ppm which occurred as a singlet. This indicates that the newly formed species is not coordinating to Rh anymore and thus must be a decomposition product of PPh_3. It was confirmed by ESI-MS that the newly formed phosphorous species was O=PPh_3.

12. References

1 C. Rieg, D. Dittmann, Z. Li, A. Kurtz, I. Lorenz, D. P. Estes, M. Buchmeiser, M. Dyballa and M. Hunger, Noble metal location in porous supports determined by reaction with phosphines, *Microporous Mesoporous Mater.*, 2021, **310**, 110594.

2 C. Rieg, D. Dittmann, Z. Li, R. Lawitzki, K. Gugeler, S. Maier, G. Schmitz, J. Kästner, D. P. Estes and M. Dyballa, Quantitative Distinction between Noble Metals Located in Mesopores from Those on the External Surface, *Chem. Eur. J.*, 2021, **27**, 17012–17023.

3 M. Dyballa, C. Rieg, D. Dittmann, Z. Li, M. Buchmeiser, B. Plietker and M. Hunger, Potential of triphenylphosphine as solid-state NMR probe for studying the noble metal distribution on porous supports, *Microporous Mesoporous Mater.*, 2020, **293**, 109778.

4 M. Kirchhof, K. Gugeler, F. R. Fischer, M. Nowakowski, A. Bauer, S. Alvarez-Barcia, K. Abitaev, M. Schnierle, Y. Qawasmi, W. Frey, A. Baro, D. P. Estes, T. Sottmann, M. R. Ringenberg, B. Plietker, M. Bauer, J. Kästner and S. Laschat, Experimental and Theoretical Study on the Role of Monomeric vs Dimeric Rhodium Oxazolidinone Norbornadiene Complexes in Catalytic Asymmetric 1,2- and 1,4-Additions, *Organometallics*, 2020, **39**, 3131–3145.